THE JOURNAL OF BIOLOGICAL CHEMISTRY
Vol. 274, No. 13, Issue of March 26, pp. 8764–8769, 1999
Printed in U.S.A.

Crystal Structure of the B Subunit of *Escherichia coli* Heat-labile Enterotoxin Carrying Peptides with Anti-herpes Simplex Virus Type 1 Activity*

(Received for publication, November 5, 1998, and in revised form, December 23, 1998)

Dubravka Matković-Calogović‡§, Arianna Loregian¶, Maria Rosa D'Acunto‡, Roberto Battistutta‡, Alessandro Tossi‖, Giorgio Palù¶, and Giuseppe Zanotti‡

From the ‡Department of Organic Chemistry and Biopolymer Research Center, University of Padova, Via Marzolo 1, 35131 Padova, Italy, the ¶Institute of Microbiology, University of Padova, Via A. Gabelli 63, 35121 Padova, Italy, and the ‖Department of Biochemistry, Biophysics and Macromolecular Chemistry, University of Trieste, Via Giorgeri 1, 34127 Trieste, Italy

Two chimeric proteins, consisting of the B subunit of *Escherichia coli* heat-labile enterotoxin with different peptides fused to the COOH-terminal ends, have been crystallized and their three-dimensional structure determined. The two extensions correspond to (*a*) a nonapeptide representing the COOH-terminal sequence of the small subunit of herpes simplex virus type 1 ribonucleotide reductase and (*b*) a 27-amino acid long peptide, corresponding to the COOH-terminal end of the catalytic subunit (POL) of DNA polymerase from the same virus. Both proteins crystallize in the $P4_12_12$ space group with one pentameric molecule per asymmetric unit, corresponding to a solvent content of about 75%. The overall conformation of the B subunit pentamer in the two chimeric proteins, which consists of five identical polypeptide chains, is very similar to that in the native AB complex and conforms strictly to 5-fold symmetry. On the contrary, the peptide extensions are essentially disordered: in the case of the nonapeptide, only 5 and 6 amino acids were, respectively, positioned in two monomers, while in the other three only 2 residues are ordered. The extension is fully confined to the surface of the pentamer opposite to the face that interacts with the membrane and consequently it does not interfere with the ability of the B subunit to interact with membrane receptors. Moreover, the conformational flexibility of the two peptide extensions could be correlated to their propensity for proteolytic processing and consequent release of a biologically active molecule into cultured cells.

Heat-labile enterotoxin (Etx)[1] is a hexameric protein produced by certain diarrheagenic strains of *Escherichia coli* and is closely related to cholera toxin in both structure and mode of action (for a review, see Ref. 1). The holotoxin has an AB_5 structure, consisting of one A subunit (EtxA, 240 amino acids, 28 kDa) which catalyzes the ADP-ribosylation and activation of the G-protein $G_s\alpha$, and five identical B monomers (EtxB, 103 amino acids, 11.6 kDa each) which are assembled in a pentameric structure and bind to the eukaryotic cell-surface receptor, monosialoganglioside GM1 (2).

The pentameric B subunit moiety of Etx can be readily purified in large quantities, and its stability, non-toxic properties, and ability to bind to ubiquitous GM1 receptors make it a potential delivery vehicle for heterologous peptides (3–5). Recently, we constructed a recombinant fusion protein (EtxB-R2) comprising the enterotoxin B subunit derived from *E. coli* H74-114 of human origin linked to the COOH-terminal 9 amino acids of the small subunit (R2) of ribonucleotide reductase of herpes simplex virus type 1 (HSV-1). The attached nonapeptide inhibits ribonucleotide reductase activity *in vitro* by disrupting the functional association between the enzyme subunits (6–8). We showed that the EtxB-R2 chimera could specifically inhibit viral replication in HSV-1-infected Vero cells, implying the EtxB-mediated delivery of the nonapeptide to the cytosol and inhibition of ribonucleotide reductase activity (5).

More recently, we also reported the construction of another recombinant toxin chimera (EtxB-Pol) derived from fusion of the *etxB* gene with a sequence encoding the 27 COOH-terminal amino acids of the catalytic subunit (POL) of HSV-1 DNA polymerase (9, 10). The carboxyl-terminal region of POL is responsible for its association with UL42, a smaller subunit which is not necessary for basal activity but increases both the rate of incorporation of deoxyribonucleotide triphosphates and the processivity of the enzyme (11, 12). The EtxB-Pol chimera retained the functional properties of both components, being able both to bind to the GM1 cell receptor like the wild type EtxB, and associate to UL42 as HSV-1 POL (10). On the basis of our data, we proposed the use of EtxB as a protein-based carrier system for the delivery of heterologous peptides in the intracellular compartment (5).

These emerging biotechnological applications of the EtxB-based chimeric toxins have highlighted the need for understanding of their three-dimensional structure. So far, the crystal structures of the AB_5 holotoxin from an *E. coli* strain of porcine origin (13–15), of its complexes with lactose (16), galactose (17), with a tumor marker disaccharide (18) and of two mutants (19, 20) are already known, along with those of the structurally related cholera toxin (21). Moreover, the crystal structure of complexes of the wild type B subunit with D-galactopyranosyl-β-D-thio-galactopyranoside and *meta*-nitrophenyl-D-galactopyranoside has been solved (22). The structures of the

* This work was supported in part by the Italian Consiglio Nazionale delle Ricerche and the Ministero dell'Università e della Ricerca Scientifica, Rome and by the AIDS Project (ISS). The costs of publication of this article were defrayed in part by the payment of page charges. This article must therefore be hereby marked "*advertisement*" in accordance with 18 U.S.C. Section 1734 solely to indicate this fact.

Atomic coordinates and structure factors (codes 1LTR and 1b44) of the EtxB-R2 and EtxB-Pol models have been deposited in the Protein Data Bank, Brookhaven National Laboratory, Upton, NY.

§ Recipient of a fellowship from the University of Padova. On leave of absence from the Laboratory of General and Inorganic Chemistry, Chemistry Dept., Faculty of Science, University of Zagreb, Ul. kralja Zvonimira 8, 10000 Zagreb, Croatia.

[1] The abbreviations used are: Etx, heat-labile enterotoxin; HSV-1, herpes simplex virus type 1; GM1, Gal(β1–3)GalNAc(β1–6)(NeuAc(α2–3))Gal(β1–6)Glc(β1–1)ceramide.

cholera toxin B subunit (23), and the structurally related *E. coli* verotoxin-1 (24) have also been published.

In this paper, the crystal structures of the EtxB-R2 and EtxB-Pol chimeric proteins at 3-Å and 3.3-Å resolution, respectively, are described. Moreover, structural characteristics are correlated with intracellular processing of chimeras and with release of biologically active peptides.

MATERIALS AND METHODS

Proteins—The hybrid EtxB-R2 protein, encoded by plasmid pAM320, was obtained by the genetic fusion of the nine COOH-terminal amino acids (YAGAVVNDL in single letter code) of the small subunit of HSV-1 ribonucleotide reductase to the *etxB* gene, as described elsewhere (5).

The EtxB-Pol fusion protein, encoded by plasmid pAL3, was created by amplifying the region of pE30 (25) corresponding to the 27 COOH-terminal amino acids of HSV-1 POL using the polymerase chain reaction and then inserting this fragment after the *etxB* gene, as reported (10).

Both EtxB-R2 and EtxB-Pol were expressed in marine non-toxinogenic *Vibrio* sp. 60 (strain MTV606, obtained from Dr. A. Ichige, University of Tokyo), and purified as reported previously (10, 26), with minor modifications.

Mass Determination—50 μg of purified EtxB-R2 protein was desalted with a Supelcosil LC318 analytical C18 column, using a gradient of 20–80% CH_3CN (0.05% trifluoroacetic acid) in 20 min. Mass spectra were measured with an electrospray ionization spectrometer (Perkin-Elmer Sciex API-1), on the sample directly eluted from the reverse phase column. Mass scans were accumulated in positive mode, with ionization and orifice voltages of 5000 V and 90 V, respectively, and a resolution of 0.1 mass units, in the 1200–2400 mass range. The mass peak reconstruct was obtained via the Fenn method (PE-Sciex, API-1 user manual).

Immunofluorescence and Microscopy—Cells for immunofluorescence were plated into 24-wells trays at a density of 6×10^4 cells per well, containing one coverslip per well and grown for 24 h. After treatment with toxin, cells were fixed with 3% paraformaldehyde in phosphate-buffered saline for 20 min at room temperature, treated with 0.27% NH_4Cl, 0.38% glycine for 10 min, and permeabilized with 0.2% saponine, 0.5% bovine serum albumin in phosphate-buffered saline for 30 min. Primary antibodies were diluted in the permeabilization medium and applied to cells for 1 h. The monoclonal antibody 118-8 anti-EtxB was kindly provided by Drs. E. Lundgren and H. Persson (University of Umea, Sweden), whereas the polyclonal antibody anti-EtxB was obtained from Dr. M. Pizza (27). The polyclonal antiserum 113 was raised against the COOH-terminal 15 residues of HSV-1 POL (28). mAb 8746 (supplied by Hilkka Lankinen, Institute of Virology, Glasgow) was raised against the YAGAVVNDL peptide. After several washes, Texas Red- or fluoresceine-conjugated secondary antibodies (from Jackson Immunoresearch Laboratories and Calbiochem, respectively) were added, incubated for a further 30 min in the same medium, and then washed. Samples were mounted in 90% glycerol, 0.2% *N*-propylgallate in phosphate-buffered saline, and observed by fluorescence microscopy. Fluorescent optical sections (1 μm thick) of cells were obtained with a Zeiss Axiovert TV-100 fluorescence microscope, equipped with a CD camera, using the Metamorph deconvolution software.

Crystallization—Crystals of EtxB-R2 and EtxB-Pol were obtained with the hanging drop method. 2 μl of protein solution, approximately 7 mg/ml, were mixed with the same volume of the precipitant solution containing 0.8 M lithium sulfate and 2% PEG 8000. The drops were equilibrated against 0.5 ml of the same precipitant solution. Needle shaped crystals of about $0.6 \times 0.2 \times 0.1$ mm^3 grew in 2–3 weeks at 4 °C, but were unstable and tended to dissolve, possibly owing to the large solvent content. Both structures crystallize in the tetragonal space group $P4_12_12$, with similar parameters of the unit cell of $a = b = 127.23$, $c = 174.19$ Å for EtxB-R2, and $a = b = 127.10$, $c = 176.10$ Å for EtxB-Pol. Structure solution has demonstrated the presence of one pentameric molecule per asymmetric unit, corresponding to V_m values (29) of 5.5 and 4.8 and to a solvent content of about 77 and 74% for EtxB-R2 and EtxB-Pol, respectively.

Structure Solution and Refinement—Despite their reasonable size, crystals did not diffract under a conventional x-ray source. Data were consequently measured at the ELETTRA synchrotron in Trieste (Italy), using an imaging plate detector system (MAR Research), with a diameter of 300 mm. Immediately before data collection the crystal was picked up with a loop, dipped for a very short time in a cryoprotectant solution, obtained by mixing 67% of the precipitant solution with 33% glycerol (v/v), and frozen in a nitrogen vapor stream at 100 K. The temperature was controlled by an Oxford Cryosystems Cryostream.

TABLE I
Statistics on data collection and processing

	EtxB-R2	EtxB-Pol
λ	1.4 Å	1.0 Å
Distance crystal-detector	300 mm	427 mm
Λφ	1°	1°
No. of frames	70	43
No. of reflections	97277	64075
No. of unique reflections	27477	16377
Resolution	23.2–3.0 Å	34.6–3.3 Å
Completeness	97.5%	74.2%
R_{merge}	0.041	0.141

D_{min}	No. of independent reflections	Completeness	Multiplicity	R_{merge}	$<I/\sigma(I)>$
(Å)		*%*			
EtxB-R2					
6.57	2601	89.4	3.1	0.043	6.9
4.74	4683	99.8	3.6	0.033	17.3
3.90	5912	100.0	3.7	0.035	15.9
3.39	6890	100.0	3.7	0.045	13.1
3.04	7391	95.6	3.4	0.073	9.1
EtxB-Pol					
7.36	1473	69.0	3.8	0.049	11.0
5.21	2656	72.4	4.1	0.100	7.2
4.26	3450	74.1	3.9	0.119	6.0
3.69	4070	74.5	3.8	0.235	3.1
3.30	4728	76.7	3.9	0.484	1.6

Data were processed with MOSFLM (30). Statistics on data collection and processing are reported in Table I. The structure of EtxB-R2 was solved with the molecular replacement technique and the AMoRe software (31) from the CCP4 suite (32), using as a template the coordinates of the B subunit of porcine *E. coli* heat-labile enterotoxin extracted from the AB_5 complex (1LTS, Ref. 14). The first five maxima of the rotation function, all related by a 5-fold symmetry, presented correlation coefficients between 13.7 and 11.6. The difference to the subsequent maximum of 11.3 was small. The highest peak of the translation function corresponded to a correlation factor of 62 and to a crystallographic *R* factor of 0.37. Despite an accurate search, it was impossible to fit a second pentameric molecule in the crystal cell. Visual inspection of the only structure solution obtained showed a reasonable three-dimensional packing, despite large holes present in the crystal lattice, and no clashes with symmetry-related molecules (Fig. 1). The structure was subjected to a rigid-body refinement procedure that brought the crystallographic *R* factor to 0.34. From this point onwards, visual inspections of the electron density maps and manual rebuilding using the TOM program (33) were alternated with automatic minimizations, for a total of 43 macrocycles. Differences in the electron density could be seen already in the first few cycles, in correspondence to residues 13 (His in human and Arg in porcine strain *E. coli* EtxB) and 46 (Ala instead of Glu). The other 2 amino acids that differ in the human and porcine strain sequences (Ser instead of Thr in position 4 and Glu instead of Lys in position 102), could not be unambiguously distinguished at this resolution. Moreover, some density was also visible close to the COOH-terminal end of each monomeric chain, corresponding to the peptide extension, but was difficult to interpret in terms of the known amino acid sequence. In the course of the refinement this density became clearer and some, but not all, residues of the extension could be fitted (see "Results and Discussion"). 116 solvent molecules were positioned as water, along with 6 sulfate ions. The final crystallographic *R* factor was 0.18 (R_{free} 0.22).

During the positional and thermal factor refinement, performed with the X-PLOR program (34, 35), non-crystallographic symmetry was imposed to main chain and side chain atoms, with different weights. The atoms corresponding to the extension were excluded from this symmetry and allowed to refine independently. They were assigned an occupancy factor of 0.75.

The molecular model determined for EtxB-R2, deprived of the amino acids corresponding to the peptide extension and of the solvent molecules, was used as the starting point for the refinement of the EtxB-Pol structure. 32 cycles of minimization performed with the X-PLOR program, alternated with inspections of the electron density maps and manual rebuilding, brought the *R* factor to 0.21 (R_{free} = 0.25). An examination of the electron density maps, however, allowed positioning

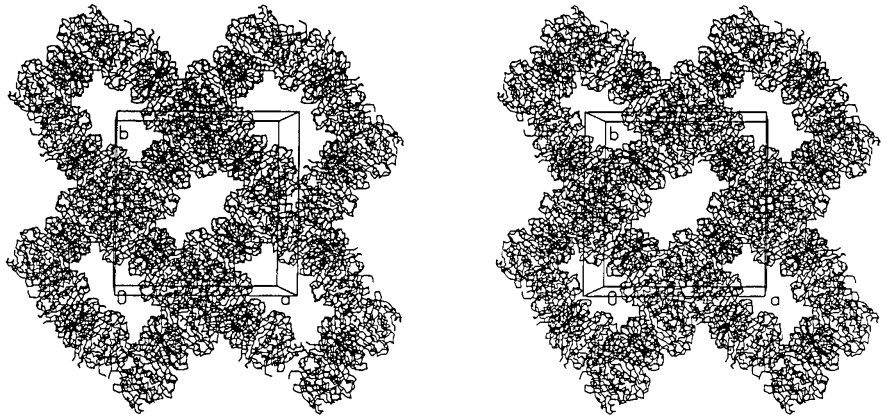

FIG. 1. **Stereo drawing of the packing of the EtxB-R2 fusion protein in the crystal cell seen along the crystallographic *c* axis.** Only Cα atoms are drawn for each molecule. A similar packing is present in the EtxB-Pol crystals.

TABLE II
Statistics on the final models of EtxB-R2 and EtxB-Pol

	EtxB-R2	EtxB-Pol
No. of unique reflections	25803 ($I>2\sigma$(I))	12394 ($I>3\sigma(I)$)
Resolution	8–3 Å	10–3.3
R_{free} test set size	7%	5%
No. of water molecules	116	0
No. of sulfate ions	6	0
Final R	0.183	0.212
Final R_{free}	0.217	0.255
Non-crystallographic symmetry		
Restraint weights		
On main chain atoms	200	200
On side chain atoms	50	50
Rool means square deviations from		
Bond lengths (Å)	0.007	0.008
Bond angles (°)	1.3	1.3

of only a few ordered amino acids. Statistics on the final models are reported in Table II.

RESULTS AND DISCUSSION

EtxB-R2—The final molecular model consists of 4230 protein atoms, 6 sulfate ions, and 116 water molecules: a control of the stereochemistry performed with the PROCHECK program (36) indicates that only 1 residue (0.2%) falls in the "disallowed" regions, 99.0% of the residues fall in "favored" or "allowed" regions, and 0.8% in the "generously allowed" regions. All the other indicators are also consistent with or better than those expected for a structure at 3-Å resolution. The only areas that are not well ordered are loop residues 54–61. A special case is represented by the peptide extension, which is discussed in detail below.

The five polypeptide chains that form the pentamer, numbered in our model from D to H (Fig. 2), assume quite a similar conformation and are related by a 5-fold non-crystallographic symmetry axis. A restraint on the non-crystallographic symmetry was imposed during the refinement, with the exception of the loop comprising residues 54–61, as differences were evident in the electron density map among different monomeric chains (Fig. 3), and for side chains involved in intermolecular contacts.

The overall conformation of the EtxB-R2 pentamer, schematically shown in Fig. 2, is very similar to the wild type EtxB pentamer of the porcine strain *E. coli* enterotoxin (14); five subunits, each consisting of two antiparallel β-sheets and two α-helices, are arranged around a central 5-fold axis. A comparison of these two pentamers gives an average root mean square deviation between our model, from residues 1 to 103, and the corresponding residues of the wild type of 0.32, 0.40, 0.44, 0.62, and 0.46 Å for monomers D to H, respectively. The only significant variation between EtxB from *E. coli* strains of porcine and

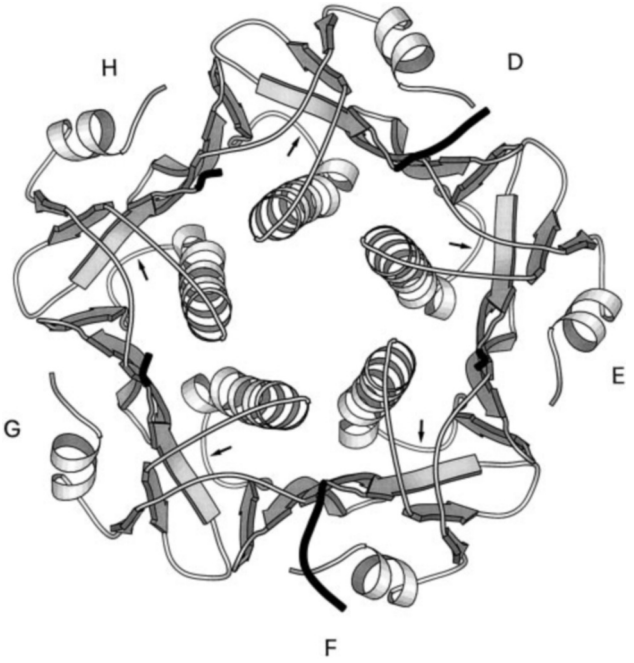

FIG. 2. **Schematic drawing of the overall structure of the EtxB-R2 pentamer, prepared with the MOLSCRIPT program (37).** The portion of peptide extensions visible in the electron density map are in *black*. *Arrows* indicate the loop 54–61. The amino acid sequences of COOH terminus of the two fusion proteins, from residue 102, are (peptide extensions in bold letters): EtxB-R2, . . . Glu-Lys-Leu-**Tyr-Ala-Gly-Ala-Val-Val-Asn-Asp-Leu;** EtxB-Pol, . . . Glu-Lys-Leu-**Ala-Gly-Phe-Gly-Ala-Val-Gly-Ala-Gly-Ala-Thr-Ala-Glu-Glu-Thr-Arg-Arg-Met-Leu-His-Arg-Ala-Phe-Asp-Thr-Leu-Ala.**

human origin is detectable around residues 54 to 61, corresponding to a solvent exposed loop. As some differences have been reported for receptor-binding specificity and antigenic determinants (38, 39), it could be proposed that these could in part depend from the exposed loop.

The amino acid sequence of our chimeric protein corresponds to the sequence of native EtxB up to position 102. Asn^{103} of the original sequence is substituted by Lys in the chimera, a Leu has been added at position 104 by the cloning procedure, and amino acids 105 to 113 correspond to the attached R2 nonapeptide (see legend to Fig. 2). This extension presents common features in all monomeric chains only for residues 103–105 (Fig. 4), as the β-strand that spans residues 95–100 in the native protein extends roughly to residue 105 in the chimera. The side chains of Lys^{103} and Tyr^{105} point toward the interior of the molecule, and Leu^{104} toward the solvent. The substitution of a polar amino acid (Asn) in position 103 with a positively charged Lys introduces a peculiar feature in the molecule: a

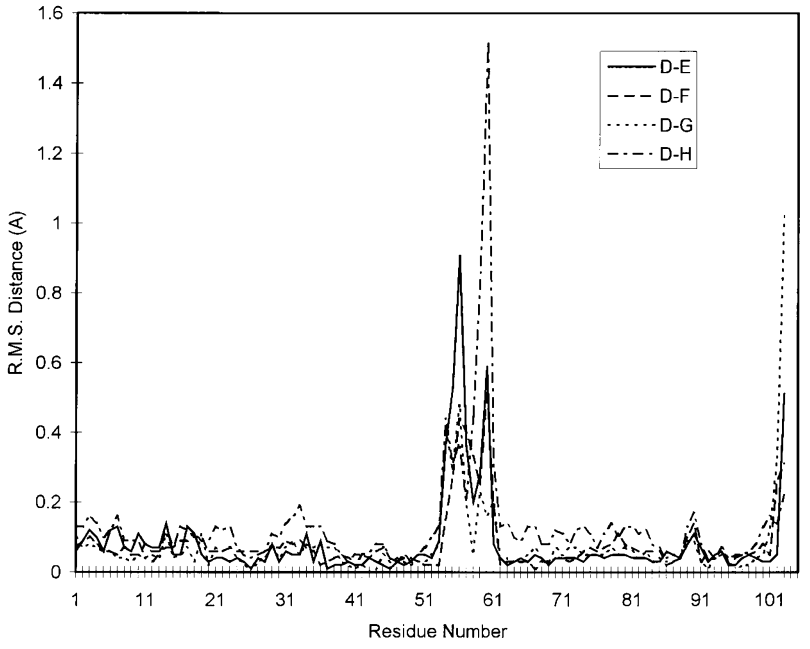

FIG. 3. **Root mean square deviations of Cα atoms of one monomer of the B subunit pentamer (residues 1–105) with respect to the other four polypeptide chains.** Significant differences are present only around residues 54–61 and from 102 to 105.

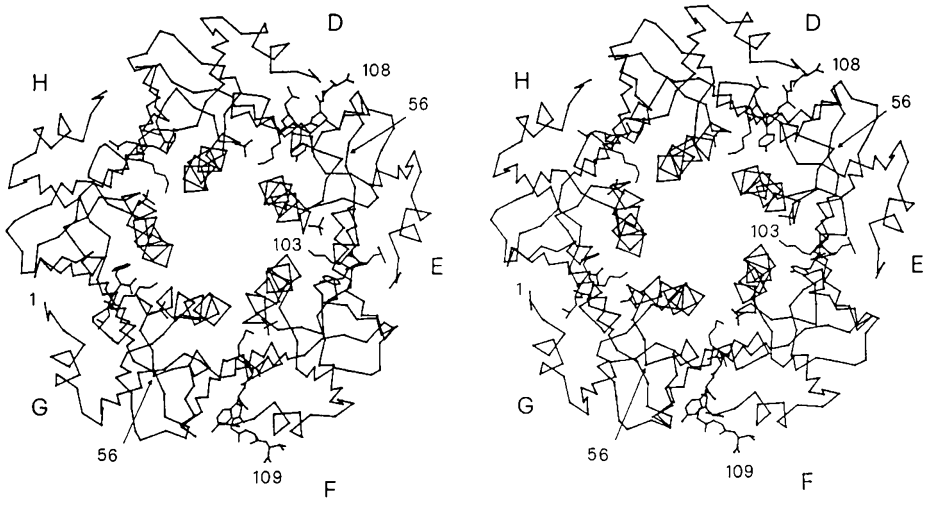

FIG. 4. **Stereo drawing of the Cα chain trace of the EtxB-R2 subunit, with all the atoms superimposed for each extension: amino acids from 103 to 108 in chain D, from 103 to 109 in chain F, from 103 to 105 in chains E, G, and H.** The five sulfate ions close to Lys^{103} are also shown.

peak of electron density, strictly obeying the molecular 5-fold symmetry, is present close to Nζ of Lys^{103} and to N of Lys^{81}. Owing to its size and to the presence of the two positive charges, it has been interpreted as a sulfate ion, due to the presence of lithium sulfate in the crystal mother liquid. We can suppose that in solution these two positive charges will be neutralized by some other negative ion. From residue 105 onwards, the situation differs in all chains. In monomers E, G, and H the remaining portion of the polypeptide could not be positioned in our model. In monomer E a large and confused density can actually be seen close to the COOH terminus and to the symmetry related molecule, but there is a gap between residue 105 and this density. For this reason, we preferred not to interpret this portion. On the contrary, in monomer D amino acids 104–108 could be positioned in the electron density map: residues 105 and 106 form a sort of tight turn, so that residues 107 and 108 continue in the reverse direction with respect to the preceding β-strand. In monomer F, the polypeptide chain is ordered up to residue 109, but in this case the final part does not make a reverse turn and can better be described as an extended chain. The reason of the different behavior of the COOH-terminal residues of the latter two chains can be found in the fact that the final part of the extension in monomer F makes close contacts with a symmetry-related pentamer.

In conclusion the entire peptide extension cannot be clearly distinguished in any of the five monomers of the chimera, and the most likely explanation is that only a few residues in the extensions are ordered in the pentamer. The eventuality that portions of the COOH-terminal chains were absent from the crystal structure due to proteolytic degradation during the purification process was excluded on the basis of mass spectrometric results. These demonstrated the presence of a single species with mass 12729.5 Da, corresponding to the theoretical mass (12730.6 Da) of an EtxB-R2 monomeric chain (Fig. 5). Moreover, it would have been difficult to reconcile proteolytic cleavage at different positions with the crystal symmetry.

An important characteristic resulting from the three-dimensional structure of the chimeric protein is that the presence of the peptide extension has no effect on the overall three-dimensional structure of the B subunit pentamer. In fact, the structure of the chimera resembles that of the B subunit pentamer bound to the A subunit in the native protein. Moreover, the extension is fully confined to the surface of the pentamer opposite to the face that interacts with the membrane (14). Thus, peptide chains that extend from the COOH-terminal end of the protein should not interfere with the ability of the B subunit

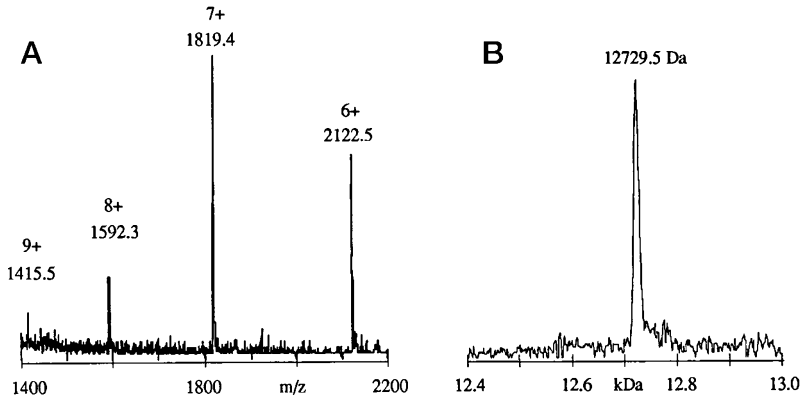

FIG. 5. **Electrospray mass spectrum (*A*) of the EtxB-R2 monomer.** The different peaks represent the indicated charge states of the molecule. The measured molecular weight is shown in the reconstructed spectrum (*B*).

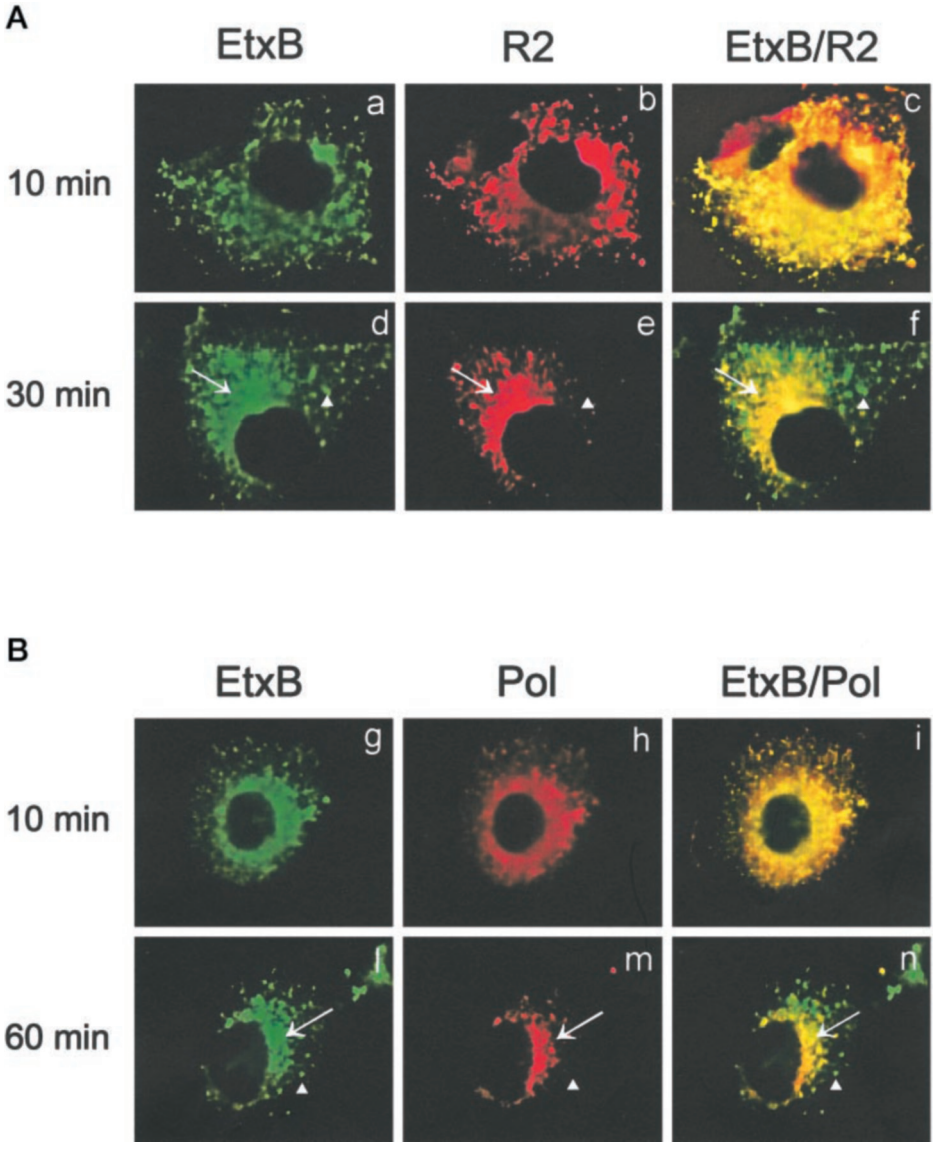

FIG. 6. **Intracellular processing of EtxB-based fusion proteins.** *A,* Vero cells were treated with EtxB-R2 for 10 min (*panels a, b*, and *c*) or 30 min (*panels d, e*, and *f*) and probed with a polyclonal antibody specific for EtxB (*EtxB*, *left panels*) and with the monoclonal antibody 8746, specific for R2 peptide (*R2, central panels*) and secondary anti-rabbit fluoresceine-conjugated or anti-mouse Texas Red-conjugated antibodies, respectively. Images were collected using a × 100 objective with a deconvolution fluorescence microscope and superimposed (*EtxB/R2, right panels*). A *yellow* color indicates colocalization of the two domains. *Arrows* and *arrowheads* point at representative EtxB+/R2+ and EtxB+/R2− compartments, respectively. *B,* Vero cells were treated with EtxB-Pol for 10 min (*panels g, h*, and *i*) or 1 h (*panels l, m*, and *n*) and probed with monoclonal antibody 118-8, specific for EtxB (*EtxB, left panels*) and with polyclonal antiserum 113, specific for POL peptide (*Pol, central panels*) and secondary anti-mouse fluoresceine-conjugated or anti-rabbit Texas Red-conjugated antibodies, respectively. Images were analyzed as described in *A*. *Arrows* and *arrowheads* point at representative EtxB+/Pol+ and EtxB+/Pol− compartments, respectively.

pentamer to interact with membrane gangliosides, as previously suggested by enzyme-linked immunosorbent assay experiments with soluble GM1 (40).

EtxB-Pol—The data for the EtxB-Pol structure were obtained only at 3.3-Å resolution and the crystal gave a weaker diffraction pattern than that of EtxB-R2, resulting in a much smaller data set. Therefore only the main features will be described. No sulfate ions could be detected and solvent molecules were not included in the model, which consists of 4191 non-hydrogen atoms. No more than 3–4 residues for each chain, corresponding to amino acids 104–107, could be safely fitted in the electron density maps. Some other electron density was visible, but not connected to the main chain and not clearly interpretable. In this case also, the B subunit pentamer maintains the doughnut-shaped structure of wild type EtxB, even if the attached POL peptide represents more than one-fourth the length of each B monomer. The 36 COOH-terminal amino acids of POL have been predicted to adopt a structure consisting of two

α-helical regions interrupted by a non-helical segment (41). We cannot exclude, owing to the quite low resolution of our electron density map, that a portion of the POL-derived peptide extension in our chimera could assume a definite conformation, despite being orientationally disordered with respect to the EtxB core.

Intracellular Processing of EtxB-R2 and EtxB-Pol—To study the intracellular fate of the two chimeras, Vero cells were treated for different times with 10 μM EtxB-R2 or EtxB-Pol and then stained either with anti-EtxB polyclonal and anti-R2 monoclonal antibodies, for EtxB-R2, or with anti-EtxB monoclonal and anti-Pol peptide antiserum, for EtxB-Pol. Analysis by deconvolution fluorescence microscopy showed that both EtxB-R2 and EtxB-Pol bound to cell surface receptors and were internalized in a manner resembling that of wild-type EtxB. These results confirm that addition of such peptides to the EtxB COOH terminus does not interfere with the receptor binding properties of either EtxB-based fusion protein in a cell system, and is consistent with our observations on the three-dimensional structure.

After 10 min incubation the two domains of both fusion proteins fully co-localized in punctated intracellular compartments which appeared either scattered throughout the cytoplasm or in the perinuclear area (Fig. 6, *A, panels a, b,* and *c* and *B, panels g, h,* and *i*), indicating that after internalization both EtxB-R2 and EtxB-Pol fusion proteins are initially intact. After 30 min the toxin and peptide portions of EtxB-Pol still co-localized (data not shown), whereas the two moieties of EtxB-R2 were beginning to dissociate: in addition to EtxB+/R2+ compartments in the perinuclear region, numerous EtxB+/R2− vesicles were visible in the surrounding cytoplasm (Fig. 6*A, panels d, e,* and *f*). A similar pattern for EtxB-Pol, with dissociation of its two components, was detectable after 1 h of treatment (Fig. 6*B, panels l, m,* and *n*).

Taken together, these results indicate that the EtxB can mediate the intracellular delivery of both R2 and Pol peptides, initially bound to EtxB and later as free molecules which are proteolytically cleaved from the toxin moiety. The decrease of the R2 signal at later times suggests that the R2 peptide may translocate in the cytosol causing a signal dilution. A complete degradation of the nonapeptide by cellular proteases should be excluded, since we previously showed that the addition of the EtxB-R2 fusion protein to virally infected Vero cells resulted in the specific inhibition of HSV-1 replication and in a reduction in dTTP levels (5), indicative of the inhibition of viral ribonucleotide reductase which is located in the cytosol. Moreover, preliminary studies demonstrated that EtxB-Pol is also active in inhibiting HSV-1 replication in Vero cells.[2]

Conclusions—The two structures presented in this article share a common conformational pattern: a highly rigid molecular core and a very flexible peptide extension. The latter is effectively floating in the solvent and is thus easily cut by a protease. This is most likely what occurs in the cell, as suggested by the fluorescence microscopy experiments. From our model, a putative site of proteolytic cleavage is located between residues 105 and 106. A break at this position would produce peptides of 8 and 26 residues, respectively, for EtxB-R2 and EtxB-Pol, with the correct sequence for interacting with the HSV-1 ribonucleotide reductase in the first case, and with DNA polymerase in the second. In fact, our data on the inhibitory activity of both EtxB-R2 (5) and EtxB-Pol[2] suggest that after intracellular proteolytic cleavage, a sufficient number of molecules of either peptide survives long enough to affect the viral target. The absence of an ordered structure for the attached peptides may thus represent an advantage, as it allows the extension to be cleaved by a cellular endoprotease, freeing it to interact with the viral target protein. In conclusion, the structural observations presented in this article further support the idea that EtxB could be used as a protein-based carrier system (5) for the intracellular delivery of heterologous peptides.

Acknowledgments—Marta Pioletti and Laura Frigotto contributed to protein purification and crystallization during their doctoral thesis. We thank the CNR staff at ELETTRA, Trieste, Italy, for help during measurements at the Crystallographic Beamline which is supported by CNR and Sincrotrone Trieste.

[2] A. Loregian, E. Papini, B. Satin, H. S. Marsden, T. R. Hirst, and G. Palu, unpublished results.

REFERENCES

1. Spangler, B. D. (1992) *Microbiol. Rev.* **56,** 622–647
2. Hirst, T. R. (1991) in *A Sourcebook of Bacterial Protein Toxins* (Alouf, J. E., and Freer, J. H., eds) pp. 75–100, Academic Press, London
3. Fergusson, L. F., McDiarmid, N., and Hirst, T. R. (1990) in *Bacterial Protein Toxins* (Rappuoli, R., Alouf, J. E., Falmagne, P., Fehrenbach, F. J., Freer, J., Gross, R., Jeljaszewicz, M., Montecucco, C., Tornasi, M., Wadstrom, T., and Witholt, B., eds) pp. 519–520, Gustav Fischer, Stuttgart
4. Nashar, T. O., Amin, T., Marcello, A., and Hirst, T. R. (1993) *Vaccine* **11,** 235–240
5. Marcello, A., Loregian, A., Cross, A., Marsden, H. S., Hirst, T. R., and Palù, G. (1994) *Proc. Natl. Acad. Sci. U. S. A.* **91,** 8994–8998
6. Dutia, B. M., Frame, M. C., Subak-Sharpe, J. H., Clark, W. N., and Marsden, H. S. (1986) *Nature* **321,** 439–441
7. Cohen, E. A., Gaudreau, P., Brazeau, P., and Langelier, Y. (1986) *Nature* **321,** 441–443
8. Paradis, H., Gaudreau, P., Brazeau, P., and Langelier, Y. (1988) *J. Biol. Chem.* **263,** 16045–16050
9. Loregian, A., Marcello, A., Hirst, T. R., Marsden, H. S., and Palù, G. (1995) *Biochem. Soc. Trans.* **23,** 61S
10. Loregian, A., Hirst, T. R., Marsden, H. S., and Palù, G. (1996) *Protein Expression Purif.* **8,** 381–389
11. Gallo, M. L., Dorsky, D. I., Crumpacker, C. S., and Parris, C. S. (1989) *J. Virol.* **63,** 5023–5029
12. Gottlieb, J., Marcy, A. I., Coen, D. M., and Challberg, M. D. (1990) *J. Virol.* **64,** 5976–5987
13. Sixma, T. K., Pronk, S. E., Kalk, K. H., Wartna, E. S., van Zanten, B. A. M., Witholt, B., and Hol, W. G. J. (1991) *Nature* **351,** 371–377
14. Sixma, T. K., Kalk, K. H., van Zanten, B. A. M., Dauter, Z., Kingma, J., Witholt, B., and Hol, W. G. J. (1993) *J. Mol. Biol.* **230,** 890–918
15. Merritt, E. A., Pronk, S. E., Sixma, T. K., Kalk, K. H., van Zanten, B. A. M., and Hol, W. G. J. (1994) *FEBS Lett.* **337,** 88–92
16. Sixma, T. K., Pronk, S. E., Kalk, K. H., Wartna, E. S., van Zanten, B. A. M., Berghuis, A. M., and Hol, W. G. J. (1992) *Nature* **355,** 561–564
17. Merritt, E. A., Sixma, T. K., Kalk, K. H., van Zanten, B. A. M., and Hol, W. G. J. (1994) *Mol. Microbiol.* **13,** 745–753
18. van den Akker, F., Steensma, E., and Hol, W. G. J. (1996) *Protein Sci.* **5,** 1184–1188
19. Merritt, E. A., Sarfaty, S., Pizza, M., Domenighini, M., Rappuoli, R., and Hol, W. G. J. (1995) *Nat. Struct. Biol.* **2,** 269–272
20. van den Akker, F., Merritt, E. A., Pizza, M. G., Domenighini, M., Rappuoli, R., and Hol, W. G. J. (1995) *Biochemistry* **34,** 10996–11004
21. Zhang, R. G., Scott, D. L., Westbrook, M. L., Nance, S., Spangler, B. D., Shipley G. G., and Westbrook, E. M. (1995) *J. Mol. Biol.* **251,** 563–573
22. Merritt, E. A., Sarfaty, S., Feil, I., and Hol, W. G. J. (1997) *Structure* **5,** 1485–1499
23. Zhang, R. G., Westbrook, M. L., Westbrook, E. M., Scott, D. L., Otwinowski, Z., Maulik, P. R., Reed, R. A., and Shipley, G. G. (1995) *J. Mol. Biol.* **251,** 550–562
24. Stein, P. E., Boodhoo, A., Tyrrell, G. J., Brunton, J. L., and Read, R. J. (1992) *Nature* **355,** 748–750
25. Stow, M. D. (1993) *Nucleic Acids Res.* **21,** 87–92
26. Loregian, A., Marcello, A., Hirst, T. R., and Palù, G. (1997) *Minerva Biotecnol.* **9,** 61–67
27. Pizza, M., Fontana, M. R., Giuliani, M. M., Domenighini, M., Magagnoli, C., Gianelli, V., Nucci, D., Hol, W., Manetti, R., and Rappuoli, R. (1994) *J. Exp. Med.* **180,** 2147–2153
28. Marsden, H. S., Murphy, M., McVey, G. L., MacEachran, K. A., Owsianka, A. M., and Stow, N. D. (1994) *J. Gen. Virol.* **75,** 3127–3135
29. Matthews, B. W. (1968) *J. Mol. Biol.* **33,** 491–497
30. Leslie, A. G. W. (1991) in *Crystallographic Computing V* (Moras, D., Podjarny, A. D., and Thierry, J. P., eds) pp. 27–38, Oxford University Press, Oxford
31. Navaza, J. (1994) *Acta Cryst. Sect. A* **50,** 157–163
32. Collaborative Computational Project Number 4 (1994) *Acta Cryst. Sect. D* **50,** 760–763
33. Jones, T. A. (1978) *J. Appl. Crystallogr.* **11,** 268–272
34. Brünger, A. T., Kuriyan, J., and Karplus, M. (1987) *Science* **235,** 458–460
35. Brünger, A. T. (1992) *Nature* **355,** 472–474
36. Laskowski, R. A., MacArthur, M. W., Moss, D. S., and Thornton, J. M. (1993) *J. Appl. Crystallogr.* **26,** 283–291
37. Kraulis, P. J. (1991) *J. Appl. Crystallogr.* **24,** 946–950
38. Olsvik, O., Lund, A., Berdal, B. P., and Bergan, T. (1983) *Natl. Instit. Public Health. Ann. (Oslo)* **6,** 5–15
39. Takeda, Y., Honda, T., Sima, H., Tsuji, T., and Miwatani, T. (1983) *Infect. Immun.* **41,** 50–53
40. Marcello, A., Loregian, A., Palù, G., and Hirst, T. R. (1994) *FEMS Microbiol. Lett.* **117,** 47–52
41. Digard, P., Williams, K. P., Hensley, P., Brooks, I. S., Dahl, C. E., and Coen, D. M. (1995) *Proc. Natl. Acad. Sci. U. S. A.* **92,** 1456–1460